TASK QUARTERLY 5 No 4 (2001), 603–610

INVESTIGATION OF SWIRLING FLOW IN DIFFUSERS INSTALLED AT THE EXIT OF AN AXIAL-FLOW PUMP

ALEXEY N. KOCHEVSKY

Department of Fluid Mechanics,
Sumy State University,
Rimsky-Korsakov 2, 40007 Sumy, Ukraine
knn@nempump.com

(Received 10 July 2001; revised manuscript received 22 August 2001)

Abstract: The swirling flow in discharge diffusers with a converging rotating hub and diverging casing is modeled by reduced Reynolds equations, and a single-sweep method is used for their solution. The flow was probed at the inlet and outlet section of these diffusers under various pump capacities and, therefore, various swirl rates. The correspondence of results in the operating range of the pump was satisfactory concerning the velocity distributions in the outlet section as well as concerning the coefficient of energy losses. The characteristic curves of the pump with different internal angles of discharge diffusers are presented and the optimal internal angle is obtained.

Keywords: axial-flow pump, discharge diffuser, axisymmetrical flow, reduced Reynolds equations, single-sweep scheme

1. Introduction

Discharge diffusers are the necessary elements of axial-flow pumps and turbines and are used for static pressure recovery and for gradual transition of flow to discharge pipes with minimal energy losses. The efficiency and overall dimensions of axial-flow machines depend a great deal on the effectiveness of discharge diffusers. The discharge diffusers are usually of conical shape, their optimal internal angles and energy losses in them depend on area ratios and swirl rates and may be evaluated according to experimental data [1, 2].

However, the diffusers in axial-flow machinery and the flow in them have geometric and kinematic features not considered in those experimental papers and need additional research. The distributions of the axial velocity as well as the velocity moment are not constant through the diffuser inlet section and are very different under various pump capacities. Besides, when a hub rotates together with an impeller, it additionally deforms these distributions. Recently, the probing of flow behind an axial-flow impeller was performed in [3], but it was restricted only to the optimal mode. Here we present results of probing the flow in a variety of operating modes.

The aim of our research is to determine for the given area ratio the internal angle α that allows us to obtain the maximal pump efficiency inside its operating range. Besides, another problem of interest is to determine how much the pump efficiency decreases with

further reduction of length of the discharge diffuser. In order to solve these problems we calculate the flow in the discharge diffuser using an appropriate mathematical model, taking as source data the obtained experimental velocity distributions at the diffuser inlet. Then we compare the numerical results with the results of probing at the diffuser outlet.

As the considered flow in the operating range of the pump is weakly swirling and mostly non-separating, we model it by discarding the highest order terms in Reynolds equations and obtaining the reduced equations of parabolic type. We calculate these equations by a single sweep in the direction of flow. More exact results may still be obtained by applying the complete Reynolds equations [4]. However, in this paper, we abstract ourselves from effects of minor importance in order to demonstrate the main physical effects that determine the flow pattern. For the same reason we use the algebraic eddy viscosity model, though for swirling flows it yields less exact results than more complex models [5].

2. Experimental research

The measurements were performed in the model axial-flow pump shown in Figure 1. The flow went from a reservoir upon the row of 5 inlet guide vanes designed to give uniform velocity moment. The exit angles of guide vanes were very large (about 84°) in order to increase the operating capacity and the flow angles behind them were from 38° near the casing wall to 53° near the hub. The 4-blade impeller with a hub ratio 0.5 was designed to obtain the non-swirling flow behind it at the nominal capacity. We have tested four discharge diffusers with an area ratio 1.72 and internal angles 12°, 24°, 40° and 90°. The angles about 90° are the worst from the point of view of energy losses, and testing the pump with such a diffuser allows the determination of the lowest value of efficiency.

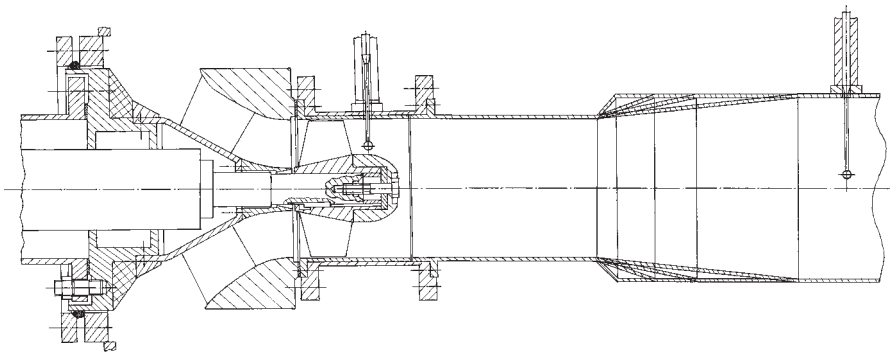

Figure 1. Model axial-flow pump

Effectiveness of discharge diffusers was evaluated, first of all, by the characteristic curves of the pump. Besides, energy losses in the discharge diffuser were calculated by the results of probing. We obtained the velocity distributions at the diffuser inlet and outlet using a 5-hole probe. The capacity calculated as a result of probing differed from the capacity measured by a diaphragm not more than by 6%. The sections of probing (the distance between them was constant) are shown in Figure 1.

3. Numerical research

The results presented below are obtained using the calculated technique described with more detail in [6]. This technique is essentially similar to the single-sweep scheme described in [7]. The main difference is the presentation of equations in the curvilinear coordinate system, in order to calculate axisymmetrical flows in annular diffusers with arbitrary wall shape. After discarding the highest order terms, the Reynolds equations and the continuity equation are as follows:

$$\frac{u}{H_1}\frac{\partial u}{\partial q_1}+\frac{v}{H_2}\frac{\partial u}{\partial q_2}-\frac{w^2}{H_1H_3}\frac{\partial H_3}{\partial q_1}+\frac{1}{H_2}\frac{\partial(\overline{u'v'})}{\partial q_2}+\frac{\overline{u'v'}}{H_1^2H_2H_3}\frac{\partial(H_1^2H_3)}{\partial q_2}=$$
$$=-\frac{1}{H_1}\frac{\partial p}{\partial q_1}+\frac{1}{\mathrm{Re}}\left(\frac{1}{H_2^2}\frac{\partial^2 u}{\partial q_2^2}+\frac{1}{H_1H_2H_3}\frac{\partial u}{\partial q_2}\frac{\partial(H_1H_3/H_2)}{\partial q_2}\right); \tag{1}$$

$$\frac{\partial p_r}{\partial q_2}=\frac{w^2}{H_3}\frac{\partial H_3}{\partial q_2}; \tag{2}$$

$$\frac{u}{H_1}\frac{\partial w}{\partial q_1}+\frac{v}{H_2}\frac{\partial w}{\partial q_2}+\frac{uw}{H_1H_3}\frac{\partial H_3}{\partial q_1}+\frac{vw}{H_2H_3}\frac{\partial H_3}{\partial q_2}+\frac{1}{H_2}\frac{\partial(\overline{v'w'})}{\partial q_2}+\frac{(\overline{v'w'})}{H_1H_2H_3^2}\frac{\partial(H_1H_3^2)}{\partial q_2}=$$
$$=\frac{1}{\mathrm{Re}}\left(\frac{1}{H_2^2}\frac{\partial^2 w}{\partial q_2^2}+\frac{1}{H_1H_2H_3}\frac{\partial w}{\partial q_2}\frac{\partial(H_1H_3/H_2)}{\partial q_2}+\frac{w}{H_1H_2}\frac{\partial}{\partial q_2}\left(\frac{H_1}{H_2H_3}\frac{\partial H_3}{\partial q_2}\right)\right); \tag{3}$$

$$\frac{1}{H_1H_2H_3}\left(u\frac{\partial(H_2H_3)}{\partial q_1}+v\frac{\partial(H_3H_1)}{\partial q_2}\right)+\frac{1}{H_1}\frac{\partial u}{\partial q_1}+\frac{1}{H_2}\frac{\partial v}{\partial q_2}=0. \tag{4}$$

where u, v, w – axial, radial and circumferential velocity components; $p = p_l(q_1) + p_r(q_1,q_2,q_3)$ – static pressure; q_1, q_2, q_3 – axial, radial and circumferential coordinates; H_1, H_2, H_3 – Lame coefficients; Re – Reynolds number.

The system of equations is closed by the condition of constant flow rate:

$$\int_0^{Q_2} u\ H_2H_3dq_2=const. \tag{5}$$

where Q_2 is the coordinate q_2 at the casing wall.

The turbulent terms are modeled using the algebraic eddy viscosity model suggested in [8] and generalised for the calculation of swirling flows in [9].

The domain is swept in the q_1 direction. At each step in this direction the w – momentum Equation (3) is calculated to obtain the circumferential velocity and the Equation (2) is calculated to obtain the radial pressure correction as it is done in [7]. However, the way of calculating the axial pressure gradient used in that paper is only acceptable for the calculation of nonseparating flows. Further steps of the algorithm are fulfilled according to [10], where a technique for calculating nonswirling separating flows is suggested, using the Flugge-Lotz approximation. The convective terms are discretised using the Newton linearisation with the coupled solution of continuity Equation (4) and u – momentum Equation (1). Axial and radial velocities and the axial pressure gradient are obtained from simultaneous solution of Equations (1), (4) and (5) using the ad hoc algorithm [10].

The computational domain is restricted with the casing, hub and sections of probing. It corresponds exactly to Figure 1, except for the following feature. Behind a blunt rotating hub

there is always a recirculation zone [11], though it is not large, it does not allow calculation of the flow by a single sweep. That is why while calculating the flow we assume that behind the rotating hub a non-rotating conical converging hub is installed. Relatively small dimensions of this imaginary hub justify the propriety of this assumption. As a result, the calculations show no reverse flow behind this hub.

4. Effectiveness criterion of the discharge diffuser

The requirement of obtaining the maximal pump efficiency is reduced to minimizing the energy losses in the discharge diffuser. As a discharge diffuser is a hydraulic element of a pump, it is convenient to refer the energy losses per time to the power N consumed by the pump in the corresponding mode (except for the idle power). So the coefficient of energy losses ξ looks as follows:

$$\xi = \frac{\int_{S_1} (p + 0.5\rho V^2) u \, dS - \int_{S_2} (p + 0.5\rho V^2) u \, dS}{N}, \tag{6}$$

where V is the total velocity, ρ is density, S_1 is the inlet section area, S_2 is the outlet section area.

As a diffuser is installed at the exit of a hydraulic machine, the kinetic energy associated with the swirl at the exit section will be irretrievably lost due to friction in a pipe or a reservoir downstream. In order to estimate this kinetic energy we introduce the coefficient of residual swirl ξ_{SW} that characterises the hydraulic losses downstream of the diffuser due to swirl decay:

$$\xi_{SW} = \frac{\int_{S_2} 0.5\rho w^2 u \, dS}{N}. \tag{7}$$

Thus, as a criterion of diffuser effectiveness we consider the total coefficient of energy losses $\xi_{SUM} = \xi + \xi_{SW}$ [6]. This coefficient characterises the energy losses inevitable in transforming the flow from the diffuser inlet to the state necessary for a customer.

5. Results

Figures 2a and 2b present the experimental distributions of axial u and circumferential w velocities behind the impeller referred to the average axial velocity at the nominal capacity. $\overline{r}$ is the current radius referred to the inlet radius of the diffuser, K_Q is the non-dimensional capacity. Markers designate the values obtained by probing, solid lines designate the distributions obtained by approximation of probed results and used as source data for the calculation of flow.

The axial velocity distribution is the most uniform at the nominal capacity. As the capacity increases, the flow is pressed to the casing, and as the capacity decreases, it is pressed to the hub. The circumferential velocity at the nominal capacity is close to zero. As the capacity increases, the flow keeps the swirl imparted by the guide vanes. As the capacity decreases, the impeller forces the flow to swirl in the opposite direction. The non-dimensional velocity w at the hub surface is about 1.3. However, as the impeller hub is rather short, its rotation has a weak influence upon the flow pattern.

The minimal and maximal capacities under which the flow was probed correspond approximately to the boundaries of the operating range of the pump. The operating range

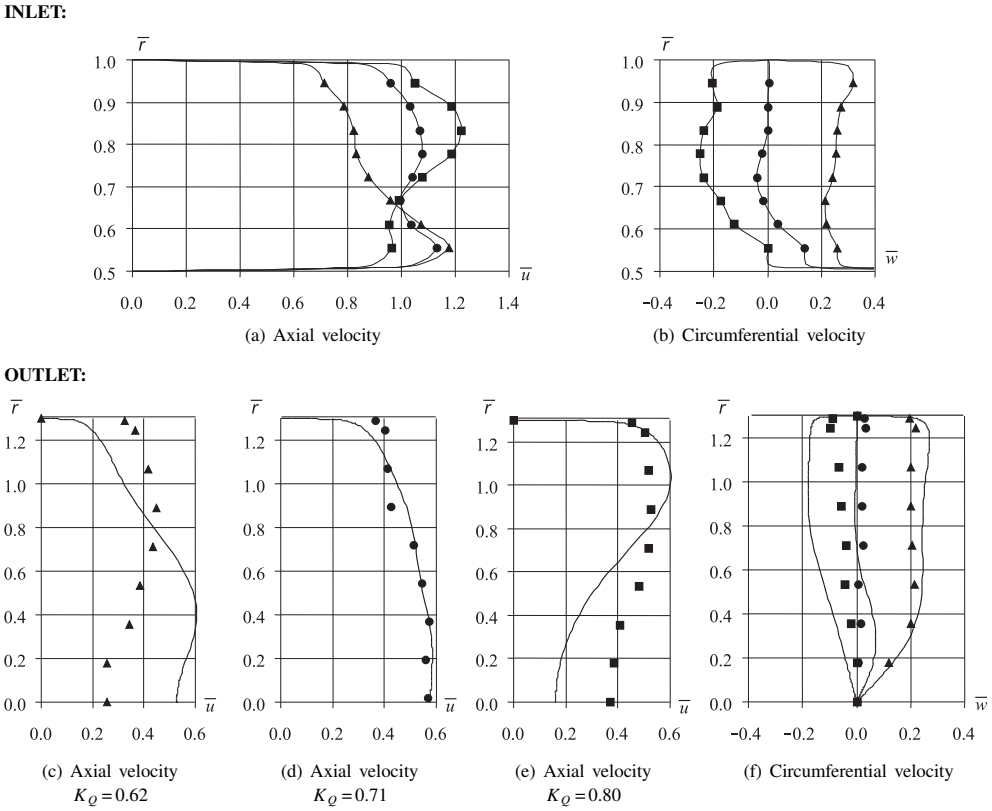

Figure 2. Velocity distributions in the inlet section (a, b) and in the outlet section (c, d, e, f) at various pump capacities: ▲ at $K_Q = 0.62$; ● at $K_Q = 0.71$; ■ at $K_Q = 0.80$ ($\alpha = 24°$)

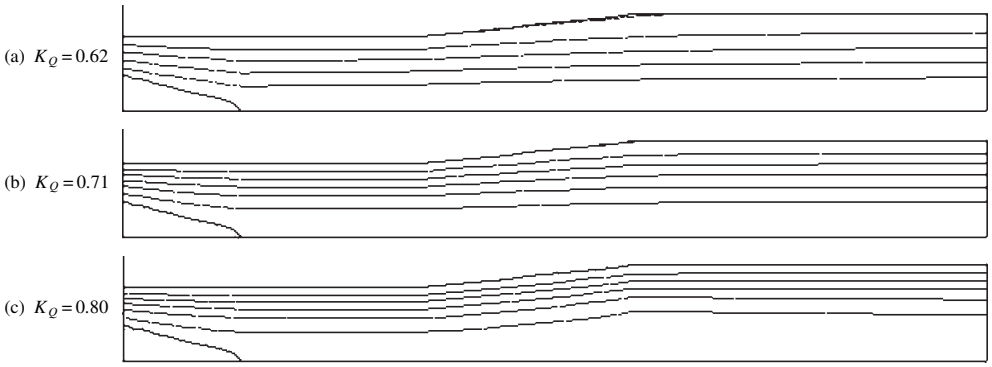

Figure 3. Calculated flow lines in the discharge diffuser ($\alpha = 24°$)

is understood as a range where the pump efficiency yields by less than 5% to the maximal value and the instability due to a pit in the head curve is not manifested. The swirl intensity at these capacities is maximal for calculating the flow by a single sweep, since the more intensive swirl causes the appearance of large recirculation zone near the axis.

In order to secure grid independent results here we use the computational grid with 101 nodes in the radial direction. The steps increase in geometric progression while moving

away from the casing and from the hub. The radial steps at the walls are about 0.001 of the inlet diameter. The axial step gradually increases from 0.01 of the diameter at the inlet to 0.05 of the diameter at the outlet.

Figure 3 shows the calculated flow lines in the computational domain of the discharge diffuser with the internal angle $\alpha = 24°$. The flow pattern is determined by velocity distribution at the inlet section. At low capacities the flow is pressed to the hub, resulting in a small separation near the casing that expands as the internal angle increases. At high capacities, on the contrary, the flow is pressed to the casing, resulting in a large wake near the axis.

Figures 2c–2f show the measured velocity distributions at the diffuser outlet with $\alpha = 24°$ and their comparison with calculated distributions at various pump capacities. Since the section of probing was situated in a certain distance from the diffuser itself, the velocity distributions were identical for all the tested diffusers. At $K_Q = 0.62$ and $K_Q = 0.80$ the axial velocity distribution has a pit near the axis due to swirl decay.

As it is seen from Figures 2c–2f, the correspondence of results is good at the nominal capacity. The most significant reasons for differences are as follows: inaccuracy of the calculation technique; inaccuracy of probing both in the inlet and outlet sections; fluctuations of the pump operating mode during the probing; possible deflections of flow from axial symmetry. As the capacity deflects from the nominal one, and the swirl intensity behind the impeller increases, the flow deflects from the assumptions of the mathematical model, and the difference between the calculated and experimental results grows.

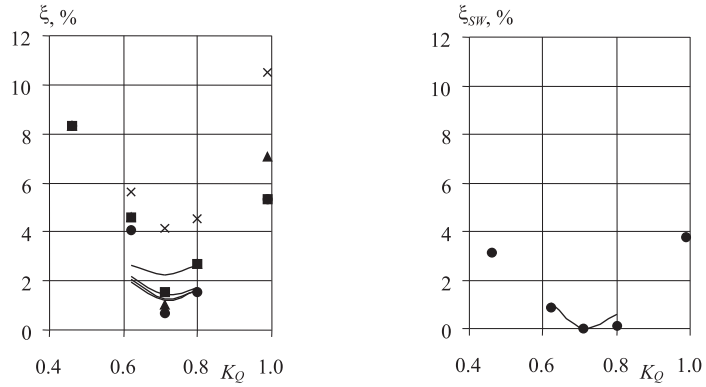

Figure 4. Dependence of coefficients of energy losses on capacity in diffusers with different internal angles α: experimental results: ▲ – 12°, ● – 24°, ■ – 40°, × – 90°; calculated results (solid lines), bottom-up: 12°, 24°, 40°, 90°

Figure 4 shows the calculated and experimental dependencies of coefficients ξ and ξ_{SW} given by Equations (6) and (7) on the capacity for each of the tested diffusers. Inaccuracy of experimental determination of absolute value ξ is rather large (about 4% of the consumed power) due to restricted accuracy of probing. But inaccuracy of experimental determination of relative value ξ is about 1% of the consumed power, since the coefficient ξ is calculated using the same velocity distributions at the inlet as well as at the outlet. The difference between losses in diffusers with different angles α was only due to the difference of wall static pressure between the sections of probing, and it was measured rather exactly.

One can see that the calculated losses are approximately equal in diffusers with $\alpha = 12°$ and $\alpha = 24°$ and increase together with α due to separation of flow. The least experimental losses are obtained in the diffuser with $\alpha = 24°$ and close results with $\alpha = 12°$ and $\alpha = 40°$, and at $\alpha = 90°$ the losses are much higher. The dependence on the internal angle α is absent at the capacity $K_Q = 0.46$ and becomes more clearly expressed as the capacity increases. Under capacities $K_Q < 0.46$ the swirl intensity behind the impeller is very strong, and the flow is pressed to periphery, preventing the separation from the casing even at large angles α.

The calculated coefficient ξ reaches minimum at the nominal capacity, where the swirl intensity is minimal, and increases together with the swirl intensity. The same result is obtained experimentally.

The coefficient ξ_{SW} demonstrates no dependence on internal angle α. It is almost equal to zero at the nominal capacity, and increases together with the swirl intensity. Figure 4 shows a good agreement between the calculated and experimental values of ξ_{SW}.

Figure 5 presents the characteristic curves of the pump at different internal angles α of the discharge diffuser. K_H is the non-dimensional head, η is the efficiency.

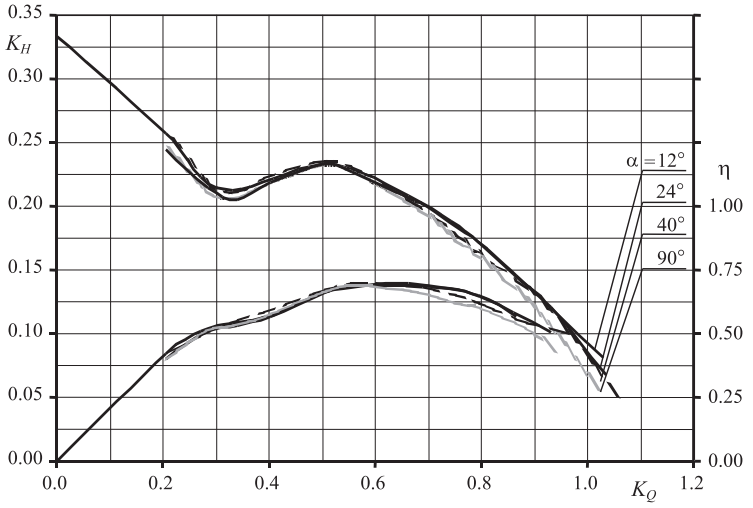

Figure 5. Characteristic curves of the pump at different angles α of the discharge diffuser

The maximal pump efficiency – 70% at the nominal capacity – is reached with the discharge diffuser with $\alpha = 24°$. Reducing the exit angles of guide vanes may increase the efficiency, but the ratio between the dependencies presented in Figure 5 will not change. As the angle α increases, the energy losses in the diffuser grow considerably due to separation, and this results in the 5% drop of efficiency at the nominal capacity, when the diffuser with $\alpha = 90°$ is installed. Under lower capacities the pump efficiency remains unchanged, but as is seen from Figure 5, the pump operation is unstable at $K_Q < 0.65$ due to a pit in the head curve.

6. Conclusion

A single-sweep method for calculating the axisymmetrical non-separating and weakly separating internal swirling flows is realised in curvilinear orthogonal coordinates. The experimental research of flow in the discharge diffuser of an axial-flow pump shows that this

technique allows the calculation of this flow with satisfactory accuracy. The best efficiency of the pump equipped with the discharge diffuser of area ratio 1.72 is reached when the internal angle of that diffuser is about 24°. When this angle is too large, the pump efficiency at the nominal capacity may drop by 5%.

Acknowledgements

The present research was conducted under leadership of Asst. Profs. A. A. Evtushenko and V. G. Nenya and under support of the collective of the Department of Fluid Mechanics.

References

[1] McDonald A T, Fox R W and Van Dewoestine R V 1971 *AIAA Journal* **9** (10) 2014
[2] Senoo Y, Kawaguchi N and Nagata T 1978 *Bulletin of the JSME* **21** (151) 112
[3] Zierke W C, Straka W A and Taylor P D 1995 *Transactions of the ASME, Journal of Fluids Engineering* **117** 485
[4] Armfield S W and Fletcher C A J 1986 *A Comparison of Single and Multi-Sweep Techniques for Reduced Navier-Stokes Equations* Comp. Tech. and Appl. CTAC 85, Amsterdam, North Holland, pp. 431 – 442
[5] Armfield S W and Fletcher C A J 1986 *Simulation of Internal Swirling Flow Using Mixing Length and k-ε Turbulence Models* Proc. Int. Symp. Comp. Fluid Dyn. in Tokyo, Amsterdam, North Holland, pp. 740 – 751
[6] Kochevsky A N 2001 *Transactions of the ASME, Journal of Fluids Engineering* **123** (in print)
[7] Armfield S W and Fletcher C A J 1986 *Int. J. Numer. Methods Fluids* **6** 541
[8] Cebeci T and Smith A O M 1974 *Analysis of Turbulent Boundary Layers* Academic Press, New York
[9] Armfield S W and Fletcher C A J 1985 *Int. J. Numer. Methods Fluids* **5** 443
[10] Kwon O K, Pletcher R H and Lewis J P 1984 *Transactions of the ASME, Journal of Basic Engineering* **106** 28
[11] Parr O 1963 *Ing. Arch.* **32** 393